Desalination and Water Treatment
www.deswater.com

doi: 10.5004/dwt.2021.27035

221 (2021) 139–151
May

Microwave induced activated carbon for the removal of metal ions in fixed-bed column study: modeling and mechanisms

Omar S.A. Al-Khazrajy[a,]*, Salam A. Mohammed[b], Omaimah Al-Musallami[b], Zahour Al-Rawahi[b], Emad Yousif[c]

[a]*Department of Chemistry, College of Education for Pure Science (Ibn al-Haytham), University of Baghdad, Baghdad Iraq, Tel. +9647715574959; email: omar.s.a@ihcoedu.uobaghdad.edu.iq*
[b]*Department of Chemical and Petrochemical Engineering, College of Engineering and Agriculture, 616 Nizwa, Sultanate of Oman, emails: salam.mohammed@unizwa.edu.om (S.A. Mohammed), 22450892@uofn.edu.om (O. Al-Musallami), 09403782@uofn.edu.om (Z. Al-Rawahi)*
[c]*Department of Chemistry, College of Science, Al-Nahrain University, Baghdad, Iraq, email: emad_yousif@hotmail.com*

Received 17 July 2020; Accepted 30 December 2020

ABSTRACT

The continuous discharge of metal-containing wastes into the aquatic system leads to a hazardous impact onto the environment and human health. This study investigated the preparation of activated carbon derived from palm-date stone using H_2SO_4 and KOH impregnation followed by microwave-induced irradiation for the adsorption of Fe^{3+}, Cd^{2+}, and Cu^{2+} from solution onto the fixed-bed column. The characterization of prepared adsorbents using scanning electron microscopy, X-ray diffraction, and Fourier transform infrared spectroscopy showed changes in the structure functional groups between adsorbents according to the used activating agent. Factors that characterize the breakthrough curves and influence the adsorption capacity including bed depth, flow rate, and initial ion concentration were studied. The maximum adsorption capacity is from 11.45 for Cd^{2+} to 85.12 mg/g for Cu^{2+} onto H_2SO_4 impregnated activated carbon (AC1). Adsorption kinetics were analyzed using Thomas, Adam–Bohart, and Yoon–Nelson models at a flow rate of 1 mL/min, bed depth of 3 cm, and initial concentrations of 12.5, 1.5, and 3.3 mg/L for Fe^{3+}, Cd^{2+}, and Cu^{2+}, respectively. Models exhibited good agreement with results experimentally obtained. Statistics showed that both KOH impregnation obtained adsorbent (AC2) and AC1 have similar ($p > 0.05$) fixed-bed adsorption performance.

Keywords: Metal ions; Activated carbon; Adsorption capacity; Breakthrough curve; Fixed-bed column

1. Introduction

The increased use of organic and inorganic chemicals has caused more spreading of hazardous substances in environment, particularly to our water systems [1,2]. One group of the contaminant is the non-biodegradable and highly toxic heavy metals [3]. Heavy metals discharge mainly from industrial and agricultural activities, leachate from landfill or naturally occur within the geochemistry structure of the catchment. They have the potential to cause harm to environment and human life even at low concentrations [4–6]. For example, it was reported that exposure to high levels of heavy metals may cause many diseases starting from oral and stomach ulcers to kidney failure and cancer [7]. Environmentally, they were found to affect the microbial community structure in soil under different contamination levels [8]. Therefore, and due to stringent regulations and water scarcity, there is a great need to develop

---

* Corresponding author.

1944-3994/1944-3986

efficient and simple approaches to remove heavy metals from waterways or discharge points.

Conventional techniques have been used for the removal of heavy metals from their aqueous solutions including coagulation, ion exchange, membrane separation, reverse osmosis, solvent extraction, chemical precipitation, and electro-flotation [9]. At concentrations lower than 10 mg/L, these methods showed high efficiency for the removal of heavy metals from their solutions but reported cost-inefficient at higher concentrations [10]. However, complications and the high cost of the treatment process increase the disadvantages of these techniques. Compare with other treatment methods, adsorption as a single step method appears to be an attractive process for the removal of heavy metals from aqueous solution [11].

Recently, the research interest has prompted towards low cost, natural, and safe materials for the purification and removal of heavy metals and other contaminants from water solutions [9,12,13]. Carbonaceous materials such as activated carbon are the widely used adsorbents for the removal of those contaminants due to their high surface area, pore structure, and high surface content of functional groups [14]. Due to low cost, adsorption of heavy metals from their solutions using activated carbon prepared from biomass, for example, bamboo [15], wheat straw [16], gooseberry seeds [17], and rice husk [18]. The palm dates by-products are highly available in the Middle East area that was used for the removal of heavy metals [2,19].

Besides, physicochemical properties of the precursors used for the preparation of activated carbon, the activation method is highly important [20]. Conventional (physical and chemical) methods for activated carbon preparation are highly used, but microwave-induced methods as alternative technology showed promising results due to its selectivity, uniform, and volumetric heating, and time and energy consuming efficiency [3,20]. On the other hand, heating using conventional methods needs a long preparation process, thus leading to greater energy consumption [21]. Moreover, in the microwave, pre-dried biomass to less than 10% is not required as in fluidized bed pyrolysis since moisture is a good adsorbent of microwave irradiation [22]. Despite the growth of microwave heating applications, there is a lack of understanding of microwave systems and the technical information for designing commercial equipment for these pyrolysis processes and no data available on the energy usage or efficiency of microwave reactors to make a compelling comparison in terms of energy balance, efficiency, and economics [21,22]. Limited research have been performed regarding the activation of biomass using a synthesis technique which combines chemical activation followed by thermal treatment using microwave-induced irradiation [3]; and up to our knowledge, less work has been done to prepare activated carbon from palm-date stones using microwave irradiation technique.

In this study, the continuous-flow fixed-bed column method was employed for metal removal from an aqueous solution. The performance of the adsorbent in this technique is described via a breakthrough curve. Many parameters including breakthrough time, which is a key to determine the operation and dynamic response of the column, the concentration of influent, flow rate, and column bed depth are affecting the saturation of adsorbents in the column and hence removal efficiency [23]. The feasibility of producing low cost activated carbon from palm-date stone as an agricultural by-product for the removal of Fe^{3+}, Cd^{2+}, and Cu^{2+} from their aqueous solutions was determined. Sulfuric acid (H_2SO_4) and potassium hydroxide (KOH) impregnation followed by microwave-induced irradiation were tested for best-activated carbon yield. Characteristics and morphology of the prepared activated carbons were also studied.

2. Materials and methods

2.1. Chemicals and reagents

All metal salts and chemicals used in this study were of >98% purity. The stock metal solutions were prepared by dissolving the calculated equivalent quantity of each metal in double-distilled water (1,000 mL). Iron(III), sulfate, and copper(II), sulfate were purchased from Scharlau (Spain). Cadmium sulfate was obtained from Merck (Germany). Sulfuric acid (H_2SO_4) and potassium hydroxide (KOH) were ordered from Sigma Aldrich (UK).

2.2. Preparation of palm-stone activated carbon

Palm-date stone was collected from the area of Nizwa, Sultanate of Oman. The preparation method was performed following Tan et al. [3] with some modifications. Briefly, collected palm-date stone was washed for several times to remove dust and fibers using distilled water and then dried at 105°C in an oven overnight. The clean product was then ground using a high-speed rotary cutting mill and sieved to <710 μm particle size. The resulted precursor was then divided into two parts. The first part was treated with H_2SO_4 while the second part was treated with KOH as activating agents at impregnation ratio (1:1, 2:1, and 3:1 w/w) for 24 h. The mixture was then dried at 105°C in an oven for 24 h. The carbonization step was carried out using microwave oven (600 W) for 15 min under nitrogen flow to remove any oxygen inside the chamber. After, the mixture was washed several times using distilled water until reached a neutral pH using Mettler–Toledo FE20 pH meter. Finally, the resulted in activated carbon was dried at 95°C for 24 h, cooled down and then kept in glass container until further characterization and analysis. The untreated carbon, activated carbon using H_2SO_4 and activated carbon using KOH were named as UC, AC1, and AC2, respectively.

2.3. Instrumental analysis and characterization

Inductively coupled plasma optical emission spectrometry (ICP-OES, PerkinElmer Optima 8000, UK) technique was applied for the measurements of metals concentrations in their aqueous solutions. The method showed low limit of detections of 0.01 mg/L (limit of quantification = 0.03 mg/L) for Cu^{2+} and Cd^{2+}. For Fe^{3+}, limit of detection was 0.1 mg/L (limit of quantification = 0.3 mg/L). All experiments and analysis were carried out in triplicate and relative standard deviation (RSD%) was found to be less than 4.2%.

Scanning electron microscopy (SEM, JEOL model JSM-65 10AL, Japan) was used for the characterization in order to have an idea about morphology of the prepared adsorbent and the images were recorded at 10 kV. The N_2 adsorption–desorption isotherm (Brunauer–Emmett–Teller (BET)) method was employed to determine the surface area of activated carbon using surface analyzer (Gemini II 2370, USA). The moisture content was estimated by drying the activated carbon in an air oven at 105°C and calculating the difference in weight. X-ray diffraction (XRD) was used to determine the possible formation of crystallographic minerals (Malvern Panalytical, UK). The analyses were performed at a scan rate of 10°/min in a 2θ range from 0° to 80°. Fourier transform infrared spectroscopy (FTIR, PerkinElmer (Spectrum GX), UK) was used in the range from 500 to 4,000 cm^{-1} to determine the functional groups on the surface of the raw and prepared activated carbons. The yield of activated carbon and ash content was calculated using the following equations [24]:

$$\text{YAC\%} = \frac{W_{\text{final}}}{W_{\text{initial}}} \times 100 \tag{1}$$

$$Y_{\text{ash}}\% = \frac{W_{\text{initial}} - W_{\text{final}}}{W_{\text{initial}}} \times 100 \tag{2}$$

where YAC represents the yield of activated carbon on dry basis after the removal of the activating agent by washing, while Y_{ash} is the yield of ash content of the activated carbon. W_{initial} and W_{final} are the weight of palm-stone and final weight of activated carbon, respectively.

2.4. Fixed-bed adsorption column

Fixed bed column experiments were performed to study the adsorption capacity of different adsorbents to remove Fe^{3+}, Cd^{2+}, and Cu^{2+} from their aqueous solutions. Approximately 1.5, 2.3, and 3.0 g of activated carbon (AC1, AC2) were packed into 1 cm diameter and 20 cm height glass column to obtain 1, 2, and 3 cm fixed bed column, respectively. A glass wool mesh was placed at the bottom of the column to prevent small particles leaking out of the column, as well as on top of the adsorbent to maintain flow rate and better distribution of the solution on the surface. A peristaltic pump was used to introduce the solutions at different flow rates (0.8, 1.0, and 1.2 mL/min) into the column at ambient temperature and variable concentrations. The effluent was collected from the bottom of the column at different time intervals. The effluent was then filtered using 0.22 μm nylon syringe filter (Gilson Scientific, UK) and analyzed for metals ions. Effect of filtration process on the recovery of the targeted metal ions was tested and found to be >98.5%, indicating no significant adsorption of the metal ions onto filter. To study the potential adsorption of the adsorbate on the wall of the column, a control treatment with the same test conditions but without the activated carbon was set up at time intervals ranging from 5 to 120 min. Finally, for the removal of adsorbed heavy metals from the column bed, an acid solution at low pH was used [25]. A solution of 0.1 M HNO_3 at a flow rate of 5 mL/min was let to pass through the column for 3 h. The resulted in solution was then analyzed for desorbed metal ions.

2.5. Fixed-bed column data analysis

Breakthrough curve integration is important to identify the adsorbent affinity to metal ions and loading behavior, by plotting the ratio of effluent (C_e (mg/L)) and influent concentrations (C_0 (mg/L)) against time (t) of flow or volume of the effluent using the non-linear regression method [25,26]. The curve describes the concentration increasing of sorbate in the effluent with the time of flow or volume of effluent. This indicates that the value of (C_e/C_0) is high at the initial step of metal ions adsorption and declines with time due to surface saturation [25]. The amounts of metal ions adsorbed on prepared activated carbons at any given time were calculated using the following equation:

$$m_{\text{ad}.t} = m_{\text{in}.t} - m_{\text{out}.t} \tag{3}$$

where $m_{\text{in}.t}$, mg is the mass of metal ions pumped into the column at t = 0 (min) and can be expressed as C_0Q_t; while $m_{\text{out}.t}$, mg is the amount of eluted metal ions from the column. Eq. (4) was used to calculate $m_{\text{out}.t}$:

$$m_{\text{out}.t} = C_0 Q \int_0^t \left(\frac{C_e}{C_0} \right) dt \tag{4}$$

where C_0 (mg/L), C_e (mg/L), Q (mL/min), and t (min) are influent concentration, effluent concentration, flow rate, and time, respectively. The column adsorption capacity was calculated in terms of breakthrough time, t_b (C_e/C_0 = 0.1) and saturation time, t_s (C_e/C_0 = 0.9) according to Eqs. (5) and (6):

$$m_{\text{ad}.t} = C_0 Q \int_0^t \left(1 - \frac{C_e}{C_0} \right) dt \tag{5}$$

$$q_{\max} = \frac{m_{\text{ad}.t}}{M} \tag{6}$$

where $q_{\max}$ (mg/g) is adsorption capacity and M (g) is mass of activated carbon packed in the column.

2.6. Kinetic models

Describing the dynamic behavior while the influent is not in a steady-state as in fixed bed column is too difficult [27]. Therefore, to predict the fixed column adsorption behavior for metal ions onto activated carbon, three kinetic models namely Thomas model, Yoon–Nelson model, and Adams–Bohart model were employed.

2.6.1. Thomas model

Thomas model is one of the highly used kinetic models that describe the behavior and performance of the adsorption process in fixed-bed column mode based on the mass transfer theory [28,29]. The model is used to calculate the theoretical adsorption capacity (q_0, mg/g) and the Thomas adsorption rate constant (K_{TH}, L/mg min) from the linear plotting of $\ln[(C_0/C_e) - 1]$ against t (min), Eq. (7):

$$\ln\left[\frac{C_0}{C_e} - 1 \right] = \frac{M q_0 K_{\text{TH}}}{Q} - K_{\text{TH}} C_0 t \tag{7}$$

where C_0 (mg/L) and C_e (mg/L) are influent and effluent concentrations, respectively.

2.6.2. Yoon and Nelson model

The simplicity of this model is one of the points that makes it highly used since the properties of the adsorbate and the surface are assumed to not affecting the adsorption [30]. This model was used to fit the breakthrough curves for the prediction of 50% breakthrough [23]. Eq. (8) is the linearized form of the model. Yoon–Nelson rate velocity constant (k_{YN}) and time needed for 50% adsorbate breakthrough (τ) can be calculated by plotting $\ln[C_e/(C_0 - C_e)]$ against t.

$$\ln\left[\frac{C_e}{C_0 - C_e}\right] = K_{\text{YN}}t - \tau K_{\text{YN}}t \quad (8)$$

2.6.3. Adams–Bohart model

The Adams–Bohart model is mainly used to describe the initial part of breakthrough curve [31]. The linearized form of the model is given in Eq. (9). Adams–Bohart rate constant (K_{AB}, L mg^{-1} min^{-1}) and equilibrium volumetric sorption capacity (N_0, mg/L) are determined from plotting $\ln[C_e/C_0]$ against t.

$$\ln\left[\frac{C_e}{C_0}\right] = K_{\text{AB}}C_0t - K_{\text{AB}}N_0\frac{Z}{\mu_0} \quad (9)$$

where Z (cm) is bed depth of the column and μ_0 (cm/min) is linear velocity of influent solution.

2.7. Statistical analysis

All adsorption and analytical experiments were performed in triplicate to ensure quality control conditions (accuracy, reliability, and reproducibility), and results represent the mean of readings. Sigmaplot 12.0 (Systat software Inc.) for processing the data and graphs. Models parameters and constants were obtained using linear regression analysis, while correlation coefficient (R^2) and t-test value ($p < 0.05$) were used to identify the best fit for adsorption system and comparison between obtained data.

3. Results and discussion

3.1. Yield and characterization of activated carbons

In this study, irradiation time, carbon, and ash content and the impregnation ratio of chemical agent and precursor were studied. Microwave irradiation time optimization was performed for AC1 and AC2 at time range of 5–15 min. The best optimal irradiation time that ensures complete carbonization for the precursor was found to be 15 min for both prepared adsorbents. Carbon and ash content, which was determined by heating 1.0 g AC1 and AC2 in a furnace oven set at 700°C for 6 h and measuring the weight loss are listed in Table 1. The ratios of yielded fixed carbon exhibited a great loss with no significant differences ($p < 0.05$) between AC1 and AC2. Different impregnation of activating agents to carbon ratios (1:1, 2:1, and 3:1 w/w) were tested and ratio of 3:1 showed the highest yield of fixed carbon. This may attributed to the decomposition of organic matter, including cellulose and lignin, with increasing the amount of chemical agents [32]. On the other hand, the decrease in fixed activated carbon for AC2 could be attributed to the higher reaction rate of carbon and KOH, which release components that are more volatile and hence increase surface area and pore volume [33].

The SEM images given in Figs. 1a and b show the differences in the surface morphology and porosity of AC1 and AC2, respectively. The high porosity of treated activated carbons reflects the high surface area. The porous structure was not highly formed in AC2 and it is clear from the figure that using sulfuric acid is a very efficient activating agent to produce activated carbons with high porosity. On the other hand, cavities and cracks on the external surface of AC2 are indicators of the high surface area [34]. This was confirmed from the results of nitrogen adsorption–desorption isotherm when AC1 and AC2 were categorized as porous materials due to their high specific surface area and total pore volume. AC1 showed surface area of 745.0 m^2/g and pore volume of 0.28 cm^3/g while AC2 exhibited higher surface area of 840.5 m^2/g and pore volume of 0.35 cm^3/g for AC2.

XRD analyses (Fig. 2) show that the synthesized activated carbons synthesized from palm date stones AC1 and AC2 have an amorphous state due to absence of sharp peak. However, little amount of two-dimensional graphite-like structure is detected in activated carbon by KOH

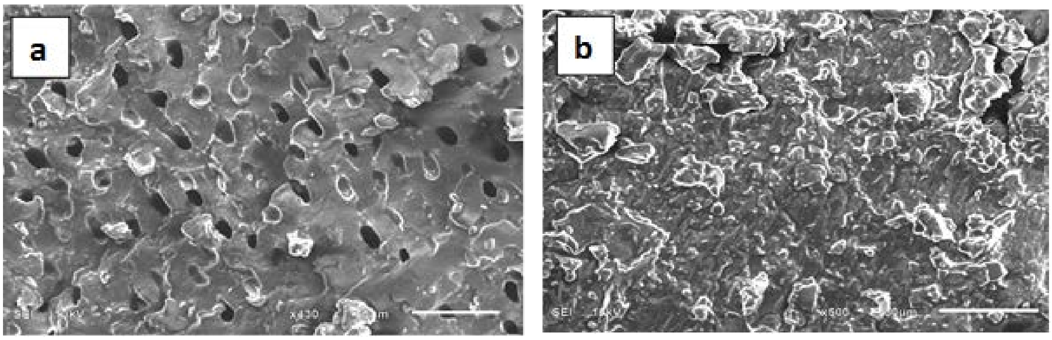

Fig. 1. SEM images of (a) H_2SO_4 treated activated carbon (AC1) and (b) KOH treated activated carbon (AC2).

Table 1
Mixing ratio, yields, and characterization of H_2SO_4 and KOH impregnation activated carbons (AC1 and AC2)

Sample	Mixing ratio (H_2SO_4/KOH:carbon)	Ash%	Fixed carbon%	Volatile carbon%	Surface area (m^2/g)	Pore volume (cm^3/g)
AC1	1:1	0.15	33.5	66.38	745.0	0.28
	2:1	0.14	34.33	65.53		
	3:1	0.13	39.41	60.46		
AC2	1:1	0.14	30.44	69.42	840.5	0.35
	2:1	0.14	31.85	68.01		
	3:1	0.12	36.41	63.47		

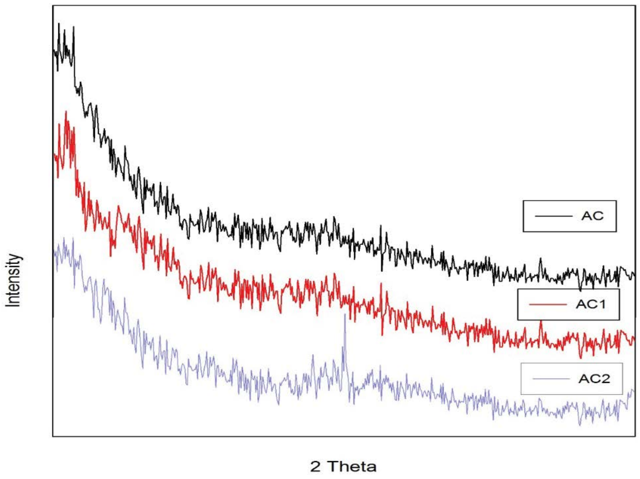

Fig. 2. XRD diffractogram of untreated carbon (UC) H_2SO_4/activated carbon (AC1) and KOH/activated carbon (AC2).

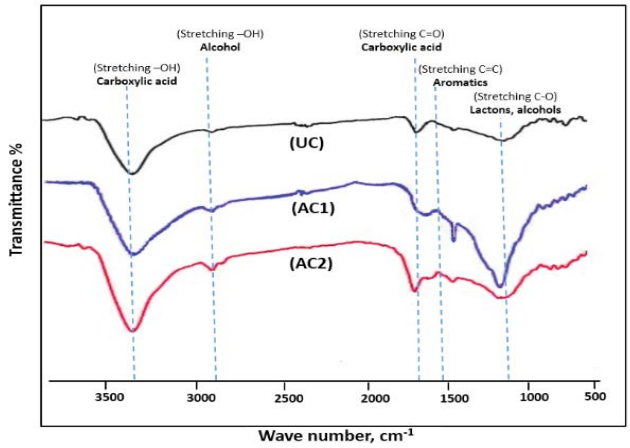

Fig. 3. FTIR spectra of untreated carbon (UC), H_2SO_4/activated carbon (AC1), and KOH/activated carbon (AC2).

(AC2) at 2θ = 44.6°, which is assigned to the plane of graphite (100). This indicates that the degree of ordered graphitization of activated carbon increases after chemical activation with KOH [33].

The FTIR spectra of untreated palm-date stones carbon and H_2SO_4/KOH activated carbon is shown in Fig. 3. The graph shows that the samples expose similar surface groups in different intensities. In all samples, the obtained band around 3,300 cm^{-1} are attributed to the presence of hydroxyl groups (hydroxyl or carboxyl). More hydroxyl functional groups (–OH) were observed in AC2 at peak observed near 3,320 cm^{-1} which is attributed to the stretching vibrations of O–H. The high intensities of the observed peaks indicate that both H_2SO_4 and KOH had dehydrated the palm-date stone and negative charge is predominant on surface. Bands at around 2,730 cm^{-1} representing stretching O–H group of phenols were of high intense for AC2 [4]. The bands at around 1,700 (UC and AC2) and 1,530 (AC1) cm^{-1} are attributed to C=O and C=C vibrations, respectively. It can be noticed from the graph that the absorptions for UC and AC1 and AC2 at 1,530 cm^{-1} are belonging to C=C stretching in aromatic rings [33]. The peaks at around 1,108 cm^{-1} are attributed to aromatic or aliphatic C–H bending vibration.

Generally, the activated carbons (AC1 and AC2) prepared using microwave-induced method showed a short time of preparation in comparison to several hours at high temperature in conventional methods when activated carbons derived from biomass are prepared [5,8,10]. Surface properties obtained here were comparable or better than those obtained elsewhere. For example, surface areas and pore sizes obtained are similar to those of 854.42 m^2/g and 0.74 cm^3/g, respectively, obtained using H_3PO_4-impregnated microwave-induced activated carbon from palm shell [3]. Moreover, AC1 and AC2 exhibited higher surface areas than those obtained using biomass origin activated carbon, for example, lentil husk (616 m^2/g) [25], fungi plant (51.2 m^2/g) [10], and water caltrop shell (264 m^2/g) [30].

3.2. Column studies

In the control treatments, no significant loss of metal ions due to adsorption to the vessels was observed with >98.8% of the initial concentrations remained at the end of time interval. Effects of flow rate, weight of column bed, and initial concentration on the breakthrough (q_b) and saturation (q_s) adsorption capacities of metals ions from their solutions onto AC1 and AC2 were studied in a fixed-bed column (Table 2). The effect of flow rates (0.8, 1.0, and 1.2 ml/min) on the removal of Fe^{3+}, Cd^{2+}, and Cu^{2+} was evaluated while the bed depth was maintained at 3.0 cm (Fig. 4). The breakthrough curves showed shifts to the left and shorter breakthrough time with increasing flow,

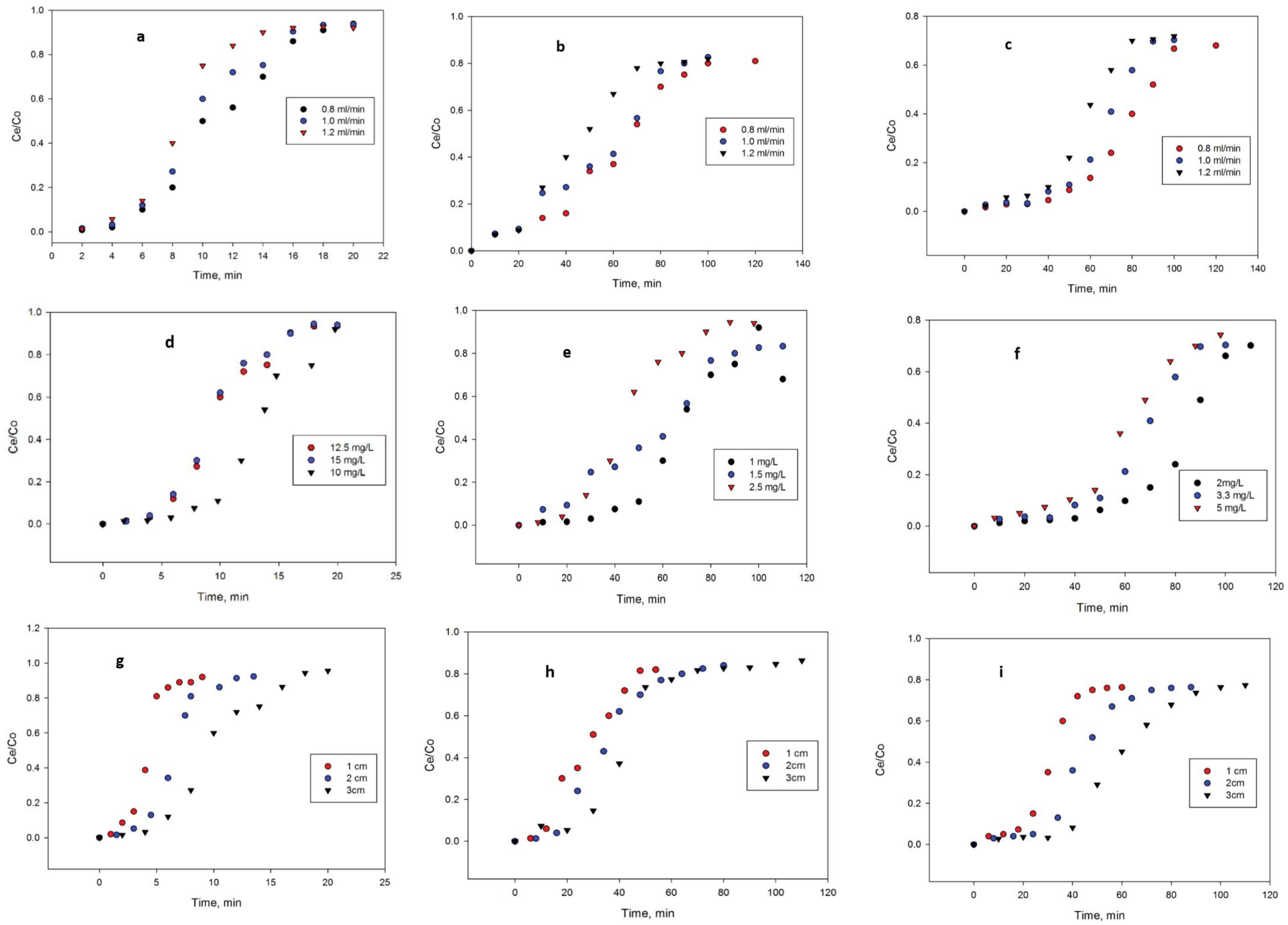

Fig. 4. Breakthrough curves of H_2SO_4/activated carbon (AC1) at different flow rates (a–c), different initial concentrations (d–f), and different bed depth (g–i).

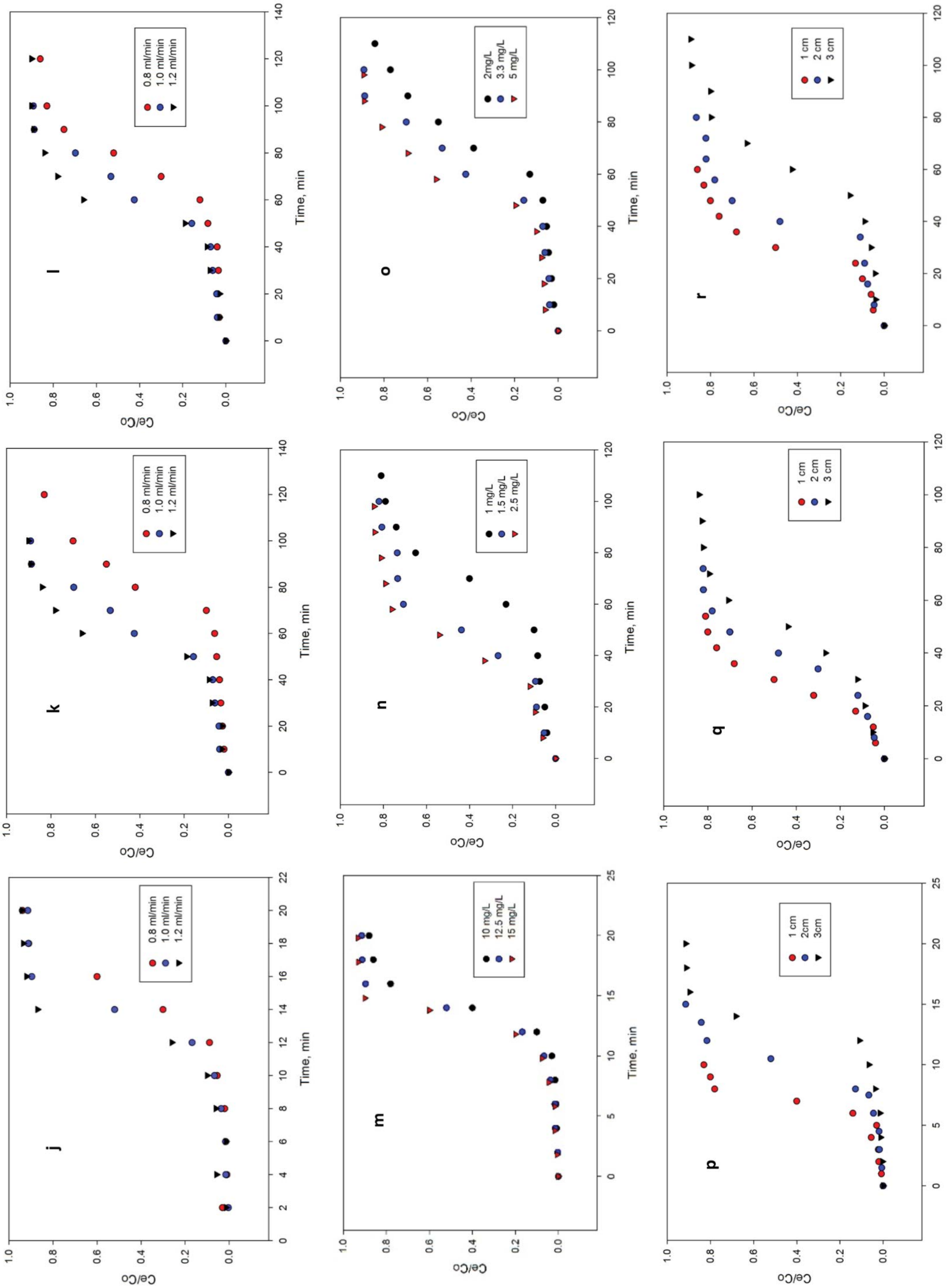

Fig. 4. Breakthrough curves of KOH/activated carbon (AC2) at different flow rates (j–l), different initial concentrations (m–o), and different bed depth (p–r).

which is related to the limited residence time of ions on the surface of the adsorbents, and then the concentration of outlet solution increases accordingly [35]. It was noticed from the graphs (Fig. 4), that the slope was high for breakthrough curve obtained at flow rate of 1.2 mL/min, which may indicate the decrease in mass transfer between the ions and the adsorbents. For example, q_b for Fe^{3+} showed around 45% decrease from 18.88 to 10.52 mg/g with increasing flow rate from 0.8 to 1.2 mL/min on AC1 (Table 2). This trend is similar to the other fixed bed adsorption studies of metal ions onto activated carbon found in literature [23,33].

The q_b and q_s at different bed depths (1, 2, and 3 cm) were also calculated, Tables 2. As noticed from Fig. 4, the breakthrough curves of Fe^{3+}, Cd^{2+}, and Cu^{2+} became more steeper and shifted from right to left as the bed depth decrease. Moreover, prolongs in breakthrough times were

Table 2
Parameters calculated from the column experimental data at different conditions for AC1 and AC2

Metal ion	Adsorbent	Conc. (mg/L)	Bed height (cm)	Flow rate (mL/min)	q_b	q_s
Fe^{3+}	AC1	12.5	3	0.8	18.88	40.46
	AC1	12.5	3	1	15.68	38.33
	AC1	12.5	3	1.2	10.52	35.10
	AC1	12.5	1	1	9.14	28.45
	AC1	12.5	2	1	12.40	37.22
	AC1	10	3	1	12.07	29.66
	AC1	15	3	1	27.02	55.32
	AC2	12.5	3	0.8	33.17	35.88
	AC2	12.5	3	1	31.32	34.44
	AC2	12.5	3	1.2	30.66	32.65
	AC2	12.5	1	1	24.5	30.20
	AC2	12.5	2	1	28.92	33.92
	AC2	10	3	1	29.20	32.22
	AC2	15	3	1	33.6	40.50
Cd^{2+}	AC1	1.5	3	0.8	16.24	24.8
	AC1	1.5	3	1	15.11	22.88
	AC1	1.5	3	1.2	12.32	21.68
	AC1	1.5	1	1	9.33	16.22
	AC1	1.5	2	1	12.55	20.34
	AC1	1	3	1	6.23	11.45
	AC1	2.5	3	1	23.95	56.42
	AC2	1.5	3	0.8	20.90	30.42
	AC2	1.5	3	1	18.80	29.32
	AC2	1.5	3	1.2	16.32	27.20
	AC2	1.5	1	1	13.52	22.66
	AC2	1.5	2	1	15.02	24.33
	AC2	1	3	1	10.88	19.18
	AC2	2.5	3	1	23.45	46.66
Cu^{2+}	AC1	3.3	3	0.8	33.52	48.56
	AC1	3.3	3	1	31.65	45.54
	AC1	3.3	3	1.2	26.45	42.35
	AC1	3.3	1	1	23.45	33.44
	AC1	3.3	2	1	28.25	43.12
	AC1	2	3	1	18.33	33.55
	AC1	5	3	1	44.32	85.12
	AC2	3.3	3	0.8	52.87	57.6
	AC2	3.3	3	1	44.23	53.40
	AC2	3.3	3	1.2	36.65	47.20
	AC2	3.3	1	1	36.66	47.21
	AC2	3.3	2	1	38.45	49.85
	AC2	2	3	1	37.10	44.20
	AC2	5	3	1	53.70	70.33

also observed with increasing bed depth for both adsorbents but more significant for AC1. The results showed increase in adsorption capacity with increasing bed depth as the adsorbent mass increasing which is due to the availability of more number of sorption sites and the sufficient diffusion time for the metal ions into the adsorbent [36]. Maximum q_b and q_s at bed depth of 3 cm, flow rate of 1 mL/min, and initial concentration of 3.3 mg/L were found to be 44.23 and 45.54 mg/g for Cu^{2+} onto AC2 and AC1, respectively (Table 2).

The effect of different initial metal ions concentrations on the breakthrough curves at a bed depth of 3 cm and flow rate of 1.0 mL/min is shown in Fig. 4. It was observed that with increasing concentration of metal ions on both adsorbent surfaces (AC1, AC2), the breakthrough time decrease and became steeper. This may related to the lower mass-transfer flux from the higher concentration solution to the surface of adsorbent. On the other hand, adsorption capacities were found to increase at high initial concentrations (Table 2); due to enhanced driving force for the diffusion of metals in the column and increase mass transfer between solution and the adsorbent [10,36]. Maximum q_b and q_s at initial Cu^{2+} concentration of 5.0 mg/L, bed depth of 3 cm, and flow rate of 1 mL/min were obtained for to be 53.7 and 85.12 mg/g onto AC2 and AC1, respectively.

For making the fixed bed reusable, 0.1 M HNO_3 solution was used to desorb targeted metal ions that have been captured onto AC1 or AC2. Higher desorption efficiencies of 89.4%, 93.4%, and 96.1% were found for Fe^{3+}, Cd^{2+}, and Cu^{2+}, respectively, onto AC2. No significant but lower efficiencies of 88.1%, 90.1%, and 94.9% were found for Fe^{3+}, Cd^{2+}, and Cu^{2+}, respectively, onto AC1. Successful desorption of adsorbed metal ions from the AC1 and AC2 fixed bed is an evidence for practical utilization of these adsorbents in the removal of heavy metals from their aqueous solutions.

3.3. Comparison of fixed bed adsorption performance of AC1 and AC2

For the aim of comparing the performance of AC1 and AC2 for the removal of metal ions from their aqueous solutions, parameters were set at flow rate of 1.0 mL/min, bed height of 3.0 cm, and initial concentration of 12.5, 1.5, and 3.3 mg/L for Fe^{3+}, Cd^{2+}, and Cu^{2+}, respectively. The patterns of adsorption breakthrough curves onto AC1 and AC2 were different for each metal ion. It can be noticed from the curves (Fig. 5), that the breakthrough time for Fe^{3+} is shorter on AC1 than AC2 whereas the q_b is significantly ($p < 0.001$) higher (2 times) for AC2 than AC1. Breakthrough curves obtained for Cu^{2+} were longer than those obtained for Fe^{3+} and Cd^{2+} on both surfaces with breakthrough adsorption capacities of 44.23 and 31.65 mg/g for AC1 and AC2, respectively. On the other hand, no significant differences ($p > 0.05$) in adsorption capacities were obtained for Cd^{2+} on both adsorbents even though breakthrough time on AC1 is shorter than that for AC2. Although AC1 shows higher q_s values than AC2 at high initial concentrations, statistical results indicated that there is no significant differences ($p > 0.05$) in q_s and hence fixed-bed adsorption performance between AC1 and AC2. Both adsorbents showed satisfactory results for the removal of selected metal ions and are beneficial for water treatment. Finally, this study obtained adsorption capacities were comparable to other studies that used activated carbon from biomass for the removal of targeted metal ions using low cost adsorbent; but most of these studies were performed in batch system. For instance, activated carbon prepared from tamarind seeds using KOH as activation agent was used for the removal of Fe^{3+} [33]. Results showed maximum adsorption capacity ranging from 0.0069 to 0.019 mg/g, which is lower than those obtained on AC1 and AC2 for Fe^{3+} in this study. For the removal of Cd^{2+}, maximum adsorption capacities in this study were within the range (31.65–74.63 mg/g) obtained using biochar derived from wheat straw [16] and higher than those (10.46 and 24.88 mg/g) using Cassava stem biochar [37]. Adsorption capacities also showed similarity to those (62.911 mg/g) resulted from removal of Cd^{2+} from aqueous solution using KOH-activated carbon from olive stone [38]. In the same study, Cu^{2+} exhibited adsorption capacity of 17.08 mg/g which is lower than capacities resulted from adsorption onto AC1 and AC2. Moreover, adsorption capacities for Cu^{2+} were found in agreement to values in the range of 21.69 to 40.05 mg/g observed using jute fiber [25], and those ranging from 37.14 to 43.47 mg/g using grape bagasse as activated carbon precursor [34].

3.4. Breakthrough curves modeling

Three kinetic models (Thomas model, Yoon–Nelson model, and Adams–Bohart model, Fig. 6) were fitted using experimental data for the determination of different parameters on the fixed-bed sorption of Fe^{3+}, Cd^{2+}, and Cu^{2+} onto AC1 and AC2. Experimental parameters were set to column depth of 2 cm, flow rate of 1.0 mL/min, and initial concentration of 12.5, 1.5, and 3.3 mg/L for Fe^{3+}, Cd^{2+}, and Cu^{2+}, respectively, as the aim is to comparing the dynamic behavior of metal ions onto prepared activated carbon surfaces.

3.4.1. Thomas model

This model highlights Langmuir kinetics of adsorption–desorption processes and describes adsorption where external and internal diffusions will not be the limiting step [25,36]. Thomas model constant (K_{TH}) and adsorption capacity of the column (q_0) for Fe^{3+}, Cd^{2+}, and Cu^{2+} adsorption onto AC1 and AC2 were obtained at selected parameters for comparison using linear regression (Eq. (7)). Thomas model fitted the experimental data with R^2 values of >0.935 and >0.923 for metal ions onto AC1 and AC2, respectively (Fig. 6). This indicates a monolayer sorption on both prepared surfaces [36]. The values (Table 3) of K_{TH} were found to decrease at high metal ion concentration (Fe^{3+}), while q_0 increased at high initial metal concentration. Under affixed conditions, K_{TH} were generally found to be higher for metal ions adsorbed onto AC1 except for Cu^{2+} which showed lower K_{TH} value (0.0112 L/min mg) for AC1 than AC1 (0.045 l/min mg), indicating more time is needed to reach the maximum adsorption [39]. The q_0 for metal ions was found to be in good agreement with values experimentally obtained for Fe^{3+} and Cu^{2+} onto AC1 while q_0 of more than 50% less for Cd^{2+}. On the other hand, no sufficient agreement between q_0 and experimental capacities for AC2 was found. The variability of q_0 on both surfaces indicating that factors other than initial concentration and flow rate controlling the adsorption process.

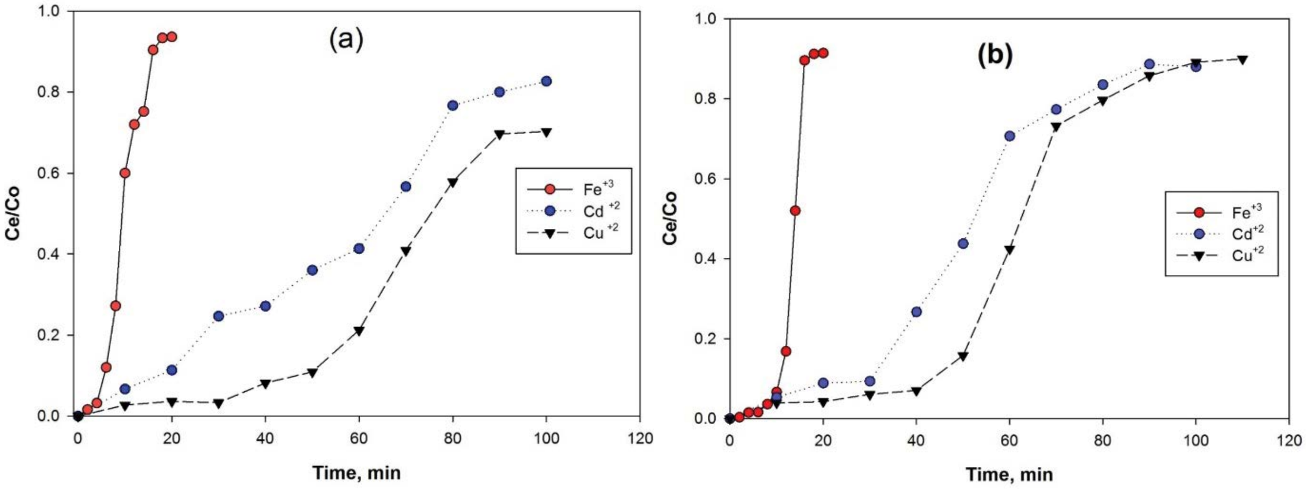

Fig. 5. Breakthrough curves of (a) H2SO4/activated carbon (AC1) and (b) KOH/activated carbon (AC2) at flow rate of 1 mL/min, bed depth of 3 cm, and initial.

Table 3
Kinetic models parameters for the removal of Fe^{3+}, Cd^{2+}, and Cu^{2+} onto AC1 and AC2 (column depth of 2 cm and flow rate of 1.0 mL/min)

Metal ion	Conc. (mg/L)	Adsorbent	Thomas model			Yoon–Nelson model			Adam–Bohart model		
			K_{TH}	q_0 (mg/g)	R^2	K_{YN}	τ	R^2	K_{AB}	N_0	R^2
Fe^{3+}		AC1	0.032	45.95	0.954	0.399	3.73	0.954	0.018	69.11	0.807
		AC2	0.039	58.23	0.959	0.489	14.33	0.959	0.026	36.88	0.953
Cd^{2+}		AC1	0.011	56.67	0.974	0.367	56.67	0.974	0.006	126.8	0.915
		AC2	0.065	11.09	0.923	0.054	60.27	0.923	0.011	45.97	0.892
Cu^{2+}		AC1	0.019	80.35	0.966	0.057	80.3	0.966	0.030	49.63	0.959
		AC2	0.045	33.77	0.958	0.067	57.28	0.958	0.028	46.76	0.942

3.4.2. Yoon-Nelson model

Based on the experimental data, K_{YN} and τ for metal ions adsorption onto AC1 and AC2 were obtained using linear regression. Results showed good fitting for data with R^2 values of >0.935 and >0.923 for metal ions onto AC1 and AC2, respectively, Table 3. Parameters (K_{YN} and τ) are known to be inversely related and the time required for 50% breakthrough (τ) decreases with increasing the initial concentration of the adsorbate [23,36,40]. This was the case in this study as metal ions of higher concentration (Fe^{3+}) showed greater K_{YN} (0.399) and smaller τ (<14.3 min) values. The values of K_{YN} showed a significant difference between Fe^{3+} and the other ions onto AC1 while Cu^{2+} showed a significant decrease in comparison to Fe^{3+} and Cd^{2+}. The low obtained K_{YN} values for Cd^{2+} and Cu^{2+} are attributed to their low concentrations in the solutions and hence slow saturation of the fixed bed [23]. However, the value of τ for Cd^{2+} and Cu^{2+} showed no significant differences for both activated carbon surfaces (AC1 and AC2).

3.4.3. Adam–Bohart model

For breakthrough curves using Adam–Bohart model (Fig. 5), respective values of N_0 and K_{AB} are presented in Table 2. From the linear regression equation results, the model was found suitable to describe the breakthrough curves for Cd^{2+} and Cu^{2+} with R^2 values of >0.942 while less satisfactory for Fe^{3+} with R^2 values of <0.806 and <0.892 for Cd^{2+} for AC1 and AC2, respectively. No significant differences in adsorption capacities (N_0) were found for metal ions onto AC2. On the other hand, Cd^{2+} showed N_0 value of 126.8 mg/L which is >2 times higher than volumetric adsorption capacity of Fe^{3+} and Cu^{2+} onto AC1. This behavior reveals that while K_{AB} values decrease, N_0 values increase at higher initial concentration [25]. Generally, the low correlation coefficient, R^2 values in comparison to the other models suggest that the Adam–Bohart model is less appropriate predictor for the breakthrough curve for Fe^{3+}, Cd^{2+}, and Cu^{2+} onto AC2.

3.5. Mechanism of interaction between metal ions and adsorbents

Understanding the mechanism of the adsorption is necessary to utilize optimal conditions and to identify the rate-limiting steps. Generally, monolayer chemisorption form is expected since adsorption followed Thomas kinetic model [25]. Results of this study revealed a broad applicability of activated carbon derived from palm-date stone in removing metal ion species; and the complexity of adsorption process suggesting the involvement of several mechanisms [38,41]. Morphology and functional groups on the surface of adsorbent are highly driving the adsorption process. From the results of FTIR, chemical impregnating using H_2SO_4 or KOH was found to increase the availability of (COOH, OH), and hence protons in oxygen functional groups [42], which is expected to control the adsorption process on the surface of AC1 and AC2. Accordingly, the main expected adsorption mechanism is cation exchange on negatively charged functional groups through the displacement of surface ions like H^+, Na^+, and Ca^{2+} with higher valence ions [10,33]. This was confirmed from the amount of Fe^{3+}, Cd^{2+}, and Cu^{2+} desorbed by HNO_3 solution, as adsorption mechanism can be explained through a desorption study [4], where metal ions were expected

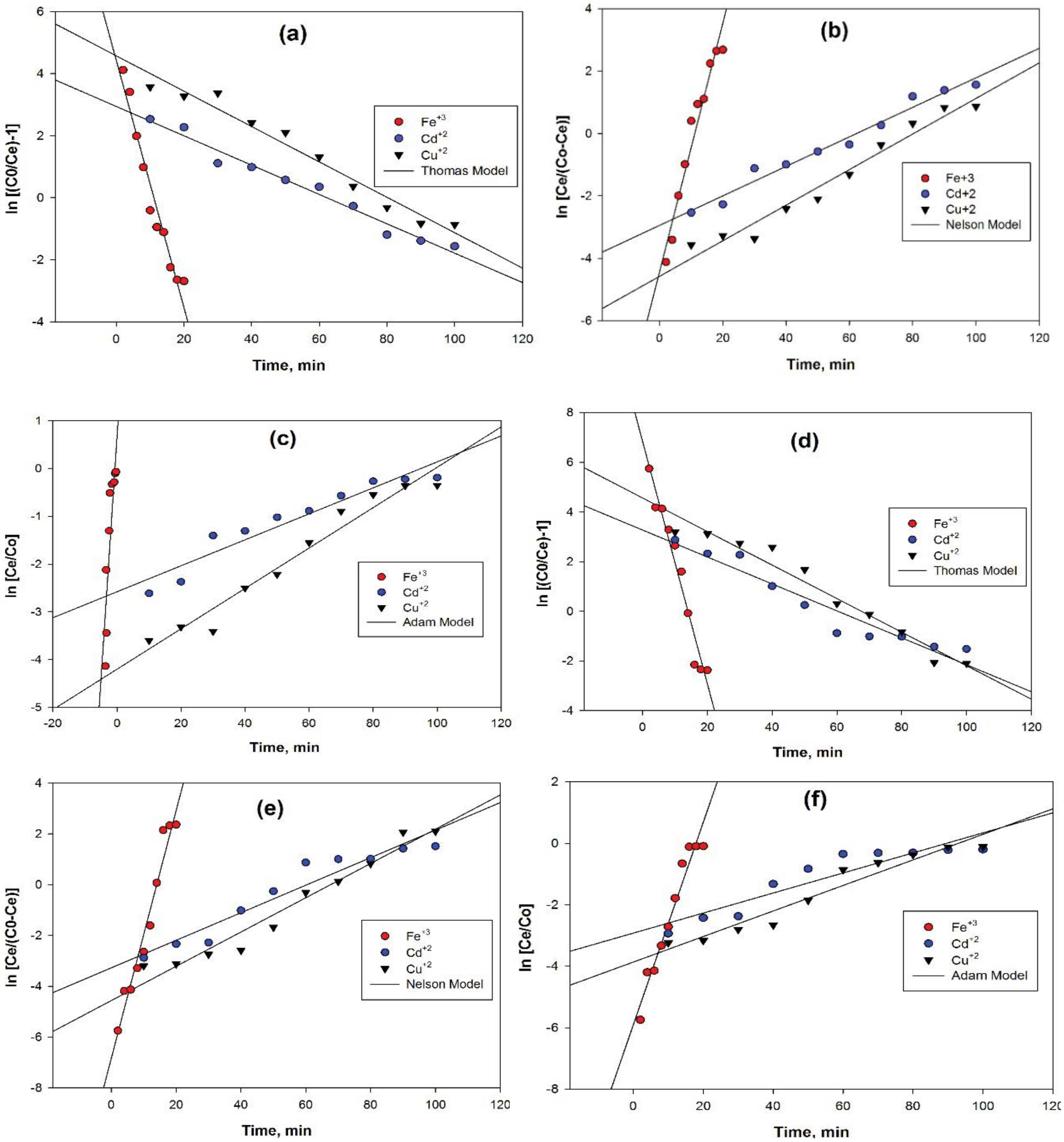

Fig. 6. Thomas model, Yoon–Nelson Model, Adam–Bohart Model for Fe^{3+}, Cd^{2+}, and Cu^{2+} onto AC1 (a–c) and AC2 (d–f) at a flow rate of 1 mL/min, bed depth of 3 cm and initial concentration of 12.5, 1.5, and 3.3 mg/L for Fe^{3+}, Cd^{2+}, and Cu^{2+}, respectively.

to be replaced by H^+. No significant differences between metal ions removal percentage from the column except for Cu^{2+} which showed higher recovery (>94.9%) on both AC1 and AC2. From the recovery results, capture mechanisms other than cation exchange may be involved. One expected mechanism is pore filling removal that was suggested for the adsorption of metal ions onto activated carbon [43]. Moreover, interaction is suggested to be *via* electrostatic interaction or π-cation interaction between aromatic rings of the activated carbon and the cation metal [44].

4. Conclusion

Activated carbon was successfully prepared from date palm stone via chemical activation using H_2SO_4 or KOH and carbonization using microwave irradiation. The resulted in activated carbons were characterized using SEM, FTIR, and XRD. It was found that AC2 is highly microporous when compared to AC1, and KOH also enhances the specific surface area and the formation of OH functional groups on the surface of activated carbon. In this study, prepared AC1 and AC2 were utilized to remove Fe^{3+}, Cd^{2+}, and Cu^{2+} from their aqueous solutions in a fixed bed reactor. The dosage, flow rate, and initial concentration were found to affect the removal efficiency. The adsorption capacity of studied metals was found to decrease in the order: $Cu^{2+} > Cd^{2+} > Fe^{3+}$. Maximum adsorption capacities of 85.12 and 70.33 mg/g were for Cu^{2+} onto AC1 and AC2, respectively at high initial concentration. Thomas kinetic model was more suitable for describing the entire breakthrough curves for metal ions on AC1 while Adam–Bohart model describes well the data obtained from removal of ions onto AC2. Thus, continuous adsorption using inexpensive and environmentally friendly activated carbon obtained from palm date stone may be considered an efficient approach for the removal of metal ions from water. Although chemical activating agents (H_2SO_4 and KOH) used in this study showed to be effective activating agents, their potential toxicity, and its implications for the environment and human health should to be taken into consideration. In the future, alternative replacements with low adverse effects need to be considered as chemical activators for the preparation of activated carbon.

Acknowledgments

The authors would like to thank the University of Nizwa, Sultanate of Oman, and the University of Baghdad, Iraq, for providing facilities and assistance in this work.

References

[1] Z. Emami, S. Azizian, Preparation of activated carbon from date sphate using microwave irradiation and investigation of its capability for removal of dye pollutant from aqueous media, J. Anal. Appl. Pyrolysis, 108 (2014) 176–184.

[2] A.M. Soliman, H.M. Elwy, T. Thiemann, Y. Majedi, F.T. Labata, N.A.F. Al-Rawashdeh, Removal of Pb(II) ions from aqueous solutions by sulphuric acid-treated palm tree leaves, J. Taiwan Inst. Chem. Eng., 58 (2016) 264–273.

[3] I.A.W. Tan, J.C. Chan, B.H. Hameed, L.L.P. Lim, Adsorption behavior of cadmium ions onto phosphoric acid-impregnated microwave-induced mesoporous activated carbon, J. Water Process Eng., 14 (2016) 60–70.

[4] H.T. Van, L.H. Nguyen, V.D. Nguyen, X.H. Nguyen, T.H. Nguyen, T.V. Nguyen, S. Vigneswaran, J. Rinklebe, H.N. Tran, Characteristics and mechanisms of cadmium adsorption onto biogenic aragonite shells-derived biosorbent: batch and column studies, J. Environ. Manage., 241 (2019) 535–548.

[5] A. Farhan, R. Jassim, N. Kadhim, The removal of zinc from aqueous solutions using Malvaparviflora, Baghdad Sci. J., 13 (2016) 482–488.

[6] O. Pourret, J.C. Bollinger, "Heavy metal" - What to do now: to use or not to use?, Sci. Total Environ., 610–611 (2018) 419–420.

[7] E. Bernard, A. Jimoh, J.O. Odigure, Heavy Metals Removal from Industrial Wastewater by Activated Carbon Prepared from Coconut Shell, 2013. Available at: www.isca.in

[8] Y. Lin, Y. Ye, Y. Hu, H. Shi, The variation in microbial community structure under different heavy metal contamination levels in paddy soils, Ecotoxicol. Environ. Saf., 180 (2019) 557–564.

[9] E. Menya, P.W. Olupot, H. Storz, M. Lubwama, Y. Kiros, Production and performance of activated carbon from rice husks for removal of natural organic matter from water: a review, Chem. Eng. Res. Des., 129 (2018) 271–296.

[10] J. Qu, T. Song, J. Liang, X. Bai, Y. Li, Y. Wei, S. Huang, L. Dong, Y. Jin, Adsorption of lead(V) from aqueous solution by modified Auricularia matrix waste: a fixed-bed column study, Ecotoxicol. Environ. Saf., 169 (2019) 722–729.

[11] A.M. Abbas, Y.I. Mohammed, T.A. Himdan, Adsorption kinetic and thermodynamic study of Congo red dye on synthetic zeolite and modified synthetic zeolite, J. Pure Appl. Sci., 28 (2015) 54–72.

[12] Q. Shi, A. Terracciano, Y. Zhao, C. Wei, C. Christodoulatos, X. Meng, Evaluation of metal oxides and activated carbon for lead removal: kinetics, isotherms, column tests, and the role of co-existing ions, Sci. Total Environ., 648 (2019) 176–183.

[13] F. Bouhamed, Z. Elouear, J. Bouzid, Adsorptive removal of copper(II) from aqueous solutions on activated carbon prepared from Tunisian date stones: equilibrium, kinetics and thermodynamics, J. Taiwan Inst. Chem. Eng., 43 (2012) 741–749.

[14] Z. Heidarinejad, O. Rahmanian, M. Fazlzadeh, M. Heidari, Enhancement of methylene blue adsorption onto activated carbon prepared from Date Press Cake by low frequency ultrasound, J. Mol. Liq., 264 (2018) 591–599.

[15] A.F. Taiwo, N.J. Chinyere, Sorption characteristics for multiple adsorption of heavy metal ions using activated carbon from Nigerian bamboo, J. Mater. Sci. Chem. Eng., 4 (2016) 39–48.

[16] M.A. Naeem, M. Imran, M. Amjad, G. Abbas, M. Tahir, B. Murtaza, A. Zakir, M. Shahid, L. Bulgariu, I. Ahmad, Batch and column scale removal of cadmium from water using raw and acid activated wheat straw biochar, Water, 11 (2019), doi: 10.3390/w11071438.

[17] S. Mondal, S.K. Majumder, Honeycomb-like porous activated carbon for efficient copper(II) adsorption synthesized from natural source: kinetic study and equilibrium isotherm analysis, J. Environ. Chem. Eng., 7 (2019), doi: 10.1016/j.jece.2019.103236.

[18] S. Sugashini, K.M.M.S. Begum, Preparation of activated carbon from carbonized rice husk by ozone activation for Cr(VI) removal, New Carbon Mater., 30 (2015) 252–261.

[19] S.A. Al-Muhtaseb, M.H. El-Naas, S. Abdallah, Removal of aluminum from aqueous solutions by adsorption on date-pit and BDH activated carbons, J. Hazard. Mater., 158 (2008) 300–307.

[20] W. Ao, J. Fu, X. Mao, Q. Kang, C. Ran, Y. Liu, H. Zhang, Z. Gao, J. Li, G. Liu, J. Dai, Microwave assisted preparation of activated carbon from biomass: a review, Renewable Sustainable Energy Rev., 92 (2018) 958–979.

[21] A.M. Abioye, F.N. Ani, Advancement in the production of activated carbon from biomass using microwave heating, J. Teknol., 79 (2017) 79–88.

[22] L. Wang, H. Lei, R. Ruan, Techno-Economic Analysis of Microwave-Assisted Pyrolysis for Production of Biofuels, Z. Fang, R. Smith Jr., X. Qi, Eds., Production of Biofuels and Chemicals with Microwave, Biofuels and Biorefineries, Springer, Dordrecht, 2015, pp. 251–263.

[23] Z. Du, T. Zheng, P. Wang, Experimental and modelling studies on fixed bed adsorption for Cu(II) removal from aqueous solution by carboxyl modified jute fiber, Powder Technol., 338 (2018) 952–959.

[24] M.B. Ahmed, M.A. Hasan Johir, J.L. Zhou, H.H. Ngo, L.D. Nghiem, C. Richardson, M.A. Moni, M.R. Bryant, Activated carbon preparation from biomass feedstock: clean production and carbon dioxide adsorption, J. Cleaner Prod., 225 (2019) 405–413.

[25] M. Basu, A.K. Guha, L. Ray, Adsorption of lead on lentil husk in fixed bed column bioreactor, Bioresour. Technol., 283 (2019) 86–95.

[26] C. Li, P. Champagne, Fixed-bed column study for the removal of cadmium(II) and nickel(II) ions from aqueous solutions using peat and mollusk shells, J. Hazard. Mater., 171 (2009) 872–878.

[27] A. Tor, N. Danaoglu, G. Arslan, Y. Cengeloglu, Removal of fluoride from water by using granular red mud: batch and column studies, J. Hazard. Mater., 164 (2009) 271–278.

[28] S. Mohan, D.K. Singh, V. Kumar, S.H. Hasan, Effective removal of fluoride ions by rGO/ZrO_2 nanocomposite from aqueous solution: fixed bed column adsorption modelling and its adsorption mechanism, J. Fluorine Chem., 194 (2017) 40–50.

[29] S. Mohan, G. Sreelakshmi, Fixed bed column study for heavy metal removal using phosphate treated rice husk, J. Hazard. Mater., 153 (2008) 75–82.

[30] Y.P. Zhang, V.S.K. Adi, H.L. Huang, H.P. Lin, Z.H. Huang, Adsorption of metal ions with biochars derived from biomass wastes in a fixed column: adsorption isotherm and process simulation, J. Ind. Eng. Chem., 76 (2019) 240–244.

[31] R. Han, Y. Wang, X. Zhao, Y. Wang, F. Xie, J. Cheng, M. Tang, Adsorption of methylene blue by phoenix tree leaf powder in a fixed-bed column: experiments and prediction of breakthrough curves, Desalination, 245 (2009) 284–297.

[32] S. Sun, Q. Yu, M. Li, H. Zhao, C. Wu, Preparation of coffee-shell activated carbon and its application for water vapor adsorption, Renewable Energy, 142 (2019) 11–19.

[33] S. Mopoung, P. Moonsri, W. Palas, S. Khumpai, Characterization and properties of activated carbon prepared from tamarind seeds by KOH activation for Fe(III) adsorption from aqueous solution, Sci. World J., 2015 (2015), doi: 10.1155/2015/415961.

[34] H. Demiral, C. Güngör, Adsorption of copper(II) from aqueous solutions on activated carbon prepared from grape bagasse, J. Cleaner Prod., 124 (2016) 103–113.

[35] W.C. Tsai, M.D.G. De Luna, H.L.P. Bermillo-Arriesgado, C.M. Futalan, J.I. Colades, M.W. Wan, Competitive fixed-bed adsorption of Pb(II), Cu(II), and Ni(II) from aqueous solution using chitosan-coated bentonite, Int. J. Polym. Sci., 2016 (2016), doi: 10.1155/2016/1608939.

[36] R. Radhika, T. Jayalatha, G. Rekha Krishnan, S. Jacob, R. Rajeev, B.K. George, Adsorption performance of packed bed column for the removal of perchlorate using modified activated carbon, Process Saf. Environ. Prot., 117 (2018) 350–362.

[37] S. Prapagdee, S. Piyatiratitivorakul, A. Petsom, Activation of cassava stem biochar by physico-chemical method for stimulating cadmium removal efficiency from aqueous solution, EnvironmentAsia, 7 (2014) 60–69.

[38] T. Bohli, A. Ouederni, I. Villaescusa, Simultaneous adsorption behavior of heavy metals onto microporous olive stones activated carbon: analysis of metal interactions, Euro-Mediterr. J. Environ. Integr., 2 (2017),doi: 10.1007/s41207-017-0030-0.

[39] L. Xu, S. Wang, J. Zhou, H. Deng, R.L. Frost, Column adsorption of 2-naphthol from aqueous solution using carbon nanotube-based composite adsorbent, Chem. Eng. J., 335 (2018) 450–457.

[40] T.M. Darweesh, M.J. Ahmed, Batch and fixed bed adsorption of levofloxacin on granular activated carbon from date (*Phoenix dactylifera* L.) stones by KOH chemical activation, Environ. Toxicol. Pharmacol., 50 (2017) 159–166.

[41] S. Biswas, U. Mishra, Continuous fixed-bed column study and adsorption modeling: removal of lead ion from aqueous solution by charcoal originated from chemical carbonization of rubber wood sawdust, J. Chem., 2015 (2015), doi: 10.1155/2015/907379.

[42] A. Kuroki, M. Hiroto, Y. Urushihara, T. Horikawa, K.I. Sotowa, J.R. Alcántara Avila, Adsorption mechanism of metal ions on activated carbon, Adsorption, 25 (2019) 1251–1258.

[43] S. Wong, N. Ngadi, I.M. Inuwa, O. Hassan, Recent advances in applications of activated carbon from biowaste for wastewater treatment: a short review, J. Cleaner Prod., 175 (2018) 361–375.

[44] E.A. Deliyanni, G.Z. Kyzas, K.S. Triantafyllidis, K.A. Matis, Activated carbons for the removal of heavy metal ions: a systematic review of recent literature focused on lead and arsenic ions, Open Chem., 13 (2015) 699–708.